Ferroelectricity of CH 3 NH 3 PbI 3 Perovskite

ARTICLE *in* JOURNAL OF PHYSICAL CHEMISTRY LETTERS · MARCH 2015

Impact Factor: 7.46 · DOI: 10.1021/acs.jpclett.5b00389

THE JOURNAL OF PHYSICAL CHEMISTRY Letters

Letter

pubs.acs.org/JPCL

Ferroelectricity of $CH_3NH_3PbI_3$ Perovskite

Zhen Fan,[†] Juanxiu Xiao,[‡] Kuan Sun,[†] Lei Chen,[†] Yating Hu,[†] Jianyong Ouyang,[†] Khuong P. Ong,[§] Kaiyang Zeng,[‡] and John Wang*[,†]

[†]Department of Materials Science and Engineering, National University of Singapore, 7 Engineering Drive 1, 117574 Singapore

[‡]Department of Mechanical Engineering, National University of Singapore, 9 Engineering Drive 1, 117575 Singapore

[§]Materials Science & Engineering Department, Institute of High Performance Computing, 1 Fusionopolis Way, 138632 Singapore

Supporting Information

ABSTRACT: Ferroelectricity has been believed to be an important but controversial origin of the excellent photovoltaic performance of organometal trihalide perovskites (OTPs). Here we investigate the ferroelectricity of a prototype OTP, $CH_3NH_3PbI_3$ ($MAPbI_3$), both theoretically and experimentally. Our first-principles calculations based on 3-D periodic boundary conditions reveal that a ferroelectric structure with polarization of ~8 $\mu C/cm^2$ is the globally stable one among all possible tetragonal structures; however, experimentally no room-temperature ferroelectricity is observed by using polarization−electric field hysteresis measurements and piezoresponse force microscopy. The discrepancy between our theoretical and experimental results is attributed to the dynamic orientational disorder of MA^+ groups and the semiconducting nature of $MAPbI_3$ at room temperature. Therefore, we conclude that $MAPbI_3$ is not ferroelectric at room temperature; however, it is possible to induce and experimentally observe apparent ferroelectric behavior through our proposed ways. Our results clarify the controversy of the ferroelectricity in $MAPbI_3$ and also provide valuable guidance for future studies on this active topic.

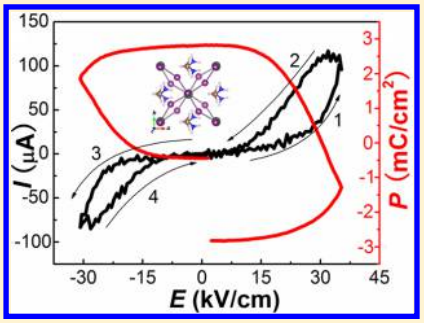

Organometal trihalide perovskites (OTPs), representing an excitingly new class of solar absorber materials, have revolutionized the photovoltaic landscape because they have demonstrated a rapid and continuous increase in power conversion efficiencies over the past 2 years from <10 to >18%.[1] The excellent photovoltaic performance of OTPs is owing to their innate desirable properties for light harvesting and charge transport, such as favorable band gap, large absorption coefficient, high dielectric constant, and long carrier diffusion length.[2−6] Among those intriguing properties of OTPs, ferroelectricity might play a key role in the efficient separation of photoexcited electron−hole pairs[7,8] and thus has attracted considerable research interest recently for both theoretical and experimental investigations.

However, the ferroelectricity in OTPs, such as that of a prototype OTP, methylammonium lead iodide ($CH_3NH_3PbI_3$, or abbreviated as $MAPbI_3$), is far from being well understood, as there have been conflicting reports. For example, through theoretical calculations, Frost et al.[7] predicted a large polarization value of 38 $\mu C/cm^2$ for $MAPbI_3$, while Zheng et al.[9] found that an antiferroelectric tetragonal structure with nearly zero polarization was more stable than its ferroelectric counterpart. Unger et al.[10−12] experimentally observed hysteresis behavior in current−voltage ($I-V$) curves and attributed it to the response of ferroelectric domains to the applied electric field. Such a hysteresis in $I-V$ curves can also originate from trapping/detrapping of charge carriers[13,14] or ion migration.[13,15] In addition, Stoumpos et al.[2,12] probed the ferroelectric behavior of $MAPbI_3$ by measuring the polarization−electric field ($P-E$) loops. Those $P-E$ loops were heavily distorted by the leakage current, which may not be regarded as convincing evidence of ferroelectricity. Recently, Kutes et al.[16] directly observed the ferroelectric domains of $MAPbI_3$ with piezoresponse force microscopy (PFM), while the phase and amplitude hysteresis loops indicating the local switching of ferroelectric domains were not shown. In a more recent work conducted by Xiao et al.,[17] no ferroelectric polarization was detected by both $P-E$ loops and PFM, which was in sharp contrast with previous reports claiming the existing of ferroelectricity in $MAPbI_3$. In this context, it would therefore be of great interest and significance to conduct a comprehensive study on the ferroelectricity of $MAPbI_3$ to clarify its existence and to further benchmark the polarization value if the ferroelectricity exists.

We have systematically studied the ferroelectricity of $MAPbI_3$ via both theoretical and experimental approaches. Viewing from the perspective of crystal structure, polar ionic displacements or ordered polar molecules are essential for ferroelectric crystals. However, the polar $CH_3NH_3^+$ (MA^+) groups are highly structurally flexible, making it difficult to determine their coordinates in the crystal cell by conventional techniques like X-ray diffraction (XRD).[18] We therefore have employed first-principles calculations to investigate the crystal structure of $MAPbI_3$,[19] taking into account the structural flexibility of MA^+

Received: February 23, 2015
Accepted: March 16, 2015

DOI: 10.1021/acs.jpclett.5b00389
J. Phys. Chem. Lett. 2015, 6, 1155−1161

groups, and to further analyze the resulting ferroelectric polarization. Experimental investigations into possible ferroelectric properties of $MAPbI_3$ have then been conducted. While the alignment of dipole moments with the applied electric field is a common feature of dielectric behavior, there are more stringent criteria of a material showing ferroelectric behavior: (i) formation of ferroelectric domains in which enough dipole moments are in the same orientation and thus inducing spontaneous polarization and (ii) switching of ferroelectric domains under an applied electric field and the presence of remnant polarization even after the applied field withdrawn. We have therefore used $P-E$ hysteresis loops to investigate the macroscopic ferroelectric switching behavior and the remnant polarization. In addition, we have employed PFM to study the ferroelectric domain structures and the local domain switching behavior. It is suggested by our calculations that on the unit-cell scale a polar structure is the most stable one among all possible tetragonal structures of $MAPbI_3$. Moreover, if 3-D periodic boundary conditions (PBCs) are satisfied, the $MAPbI_3$ bulk is expected to yield a ferroelectric polarization of $\sim 8\ \mu C/cm^2$; however, no sign of room-temperature ferroelectric behavior is observed experimentally through $P-E$ loops or PFM. The reasons of the discrepancy between our theoretical and experimental results are discussed in terms of the dynamic orientational disorder of MA^+ groups and the semiconducting nature of $MAPbI_3$ at room temperature. Finally, we propose several possible pathways to induce and experimentally observe apparent ferroelectric behavior of $MAPbI_3$.

We performed density functional theory (DFT) calculations with the PBEsol[20] exchange-correlation functional as implemented in the Vienna ab initio simulation package (VASP), which employs the projected-augmented wave (PAW) method. The orbitals of $5d^{10}6s^26p^2$, $5s^25p^5$, $2s^22p^3$, $2s^22p^2$, and $1s^1$ were explicitly treated as valence electrons for Pb, I, N, C, and H, respectively. Brillouin zone integrations were performed using a Gaussian broadening of 0.1 eV, a $3 \times 3 \times 2$ Monkhorst–Pack grid of k-points, and an energy cutoff of 400 eV for plane waves. We adopted tetragonal cells and fixed lattice parameters to typical experimental data,[18] that is, $a = b = 8.8$ Å and $c = 12.685$ Å. The Pb and I atoms were initially placed at those positions following the tetragonal *I4/mcm* symmetry.[18] Eighteen different initial configurations of MA^+ groups depending on the orientation of C–N bonds and the rotation of H tetrahedrons were fully considered. During the structure optimization, all atoms in the $MAPbI_3$ system were relaxed toward equilibrium until the Hellmann–Feynman forces were <0.01 eV/Å.

The perovskite $MAPbI_3$ thin films were prepared following our previous report with slight modifications.[21] In brief, precursor solution was prepared by dissolving 1.4 M PbI_2 and 1.4 M methylammonium iodide in a cosolvent of dimethyl sulfoxide (DMSO) and γ-butyrolactone (GBL) (vol. ratio = 3/7) at 60 °C overnight. PEDOT:PSS (poly(3,4-ethylenedioxythiophene)/polystyrenesulfonate, Clevios P VP AI 4083) was spin-cast onto a clean indium tin oxide (ITO) glass at 8000 rpm to form the substrate. Both the precursor solution and the substrate were preheated at 85 °C on a hot plate inside a glovebox filled with dry nitrogen. The hot precursor solution was spin-coated onto the hot substrate at 1000 rpm for 20 s and then at 3500 rpm for 60 s. At 50 s after the spin coating started, the wet spinning film was quenched by 1 mL of anhydrous toluene. The as-cast films were annealed at 100 °C for 20 min inside the glovebox. The $MAPbI_3$ thin films were stored in nitrogen-filled vials and taken out of the glovebox for characterizations. The crystal structure analysis of our films was done by powder XRD (Bruker D8 Advanced). The macroscopic $P-E$ hysteresis measurements were conducted by using the Radiant Precision Workstation (Radiant Technologies). The ferroelectric domain structures were investigated by PFM using an SPM system (MFP-3D, Asylum Research) with a software platform (IGOR PRO 6.12A) and an SPM control software (Asylum Research). A commercially available Pt-coated Si tip (AC240TM, Olympus) was employed. The amplitude of AC voltage used for detecting the ferroelectric domains was set to be 0.5 V. The local amplitude and phase hysteresis loops were studied by piezoresponse force spectroscopy (PFS).

As can be seen from Figure S1a (Supporting Information), when viewed from the *c* axis, the neighboring C–N bonds in both [001] and [110] directions exhibit three different orientations, that is, parallel, antiparallel, and crossed. In addition, H tetrahedrons are free to rotate and can face toward either $+c$ (upward) or $-c$ (downward) axis. Therefore, we construct 18 initial tetragonal structures to ensure the comprehensiveness. Interestingly, after optimizing all atomic positions, those initial structures all reach local energy minima and thus result in 18 different final structures (Figure S1b–s, Supporting Information). This observation confirms that the crystal structure of $MAPbI_3$ is extremely sensitive to the orientation and rotation of MA^+ groups. It also indicates that in the DFT calculations of $MAPbI_3$ one should be very careful with the optimized structure because it might be a locally stable one rather than the globally stable one that is actually needed. The calculated energies of all tetragonal structures are shown in Table 1. The globally stable tetragonal structure is found to be

Table 1. Relative Total Energies per 48-Atom Unit Cell (E_t) of 18 Possible Tetragonal Structures of $MAPbI_3$[a]

label	E_t (meV)	label	E_t (meV)	label	E_t (meV)
T-1	53.6	T-2	93.6	T-3	91.8
T-4	94.6	T-5	117.5	T-6	166.9
T-7	121.0	T-8	110.5	T-9	134.7
T-10	83.5	T-11	104.5	T-12	100.6
T-13	0.0	T-14	61.0	T-15	15.1
T-16	87.4	T-17	7.2	T-18	66.1

[a]Structures corresponding to the labels in the Table are visualized in Figure S1 (Supporting Information).

T-13; however, the energies of T-13, T-15, and T-17 are quite close. To further confirm that T-13 is more stable than the other two, we performed a finer structural optimization with a $6 \times 6 \times 5$ *k*-mesh and an energy cutoff of 500 eV, and consistent results were obtained (not shown here). In addition, the calculated relative energies of all structures were further verified with van der Waals corrections, which yielded similar results (Table S1 in Supporting Information). Figure 1a,b shows the structure of T-13, where the neighboring C–N bonds get crossed in both [001] and [110] directions (viewed from the *c* axis), all MA^+ dipoles point toward the $+a$ (or equivalently $-a$, $+b$, and $-b$) axis, and all H tetrahedrons with C centers face toward the $+c$ (or equivalently $-c$) axis. In this structure, as shown in Figure 1c, the MA^+ dipole significantly tilts out of the *aob* plane and the NH_3 component is strongly pulled close to the surrounding iodine ions, which is consistent with previous findings.[18,22] This is because compared with CH_3, NH_3 is more positively charged and exhibits stronger hydrogen bonds with

DOI: 10.1021/acs.jpclett.5b00389
J. Phys. Chem. Lett. 2015, 6, 1155–1161

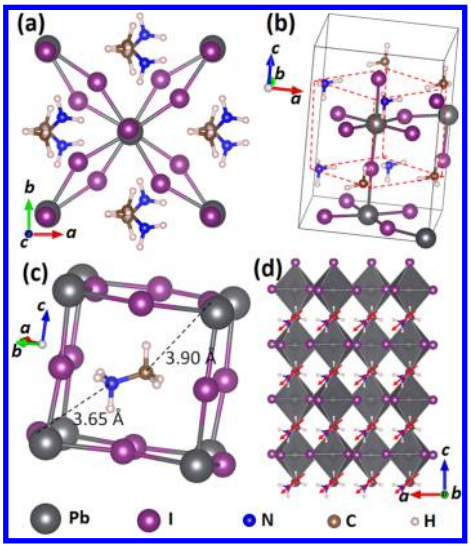

Figure 1. Most stable tetragonal structure of $MAPbI_3$ (T-13) viewed from (a) *c* axis and (b) an arbitrary axis. The red dotted line in panel b characterizes a pseudocubic primitive cell of perovskite ABX_3. (c) The tilt and shift of MA^+ molecule within the PbI_3^- cage. (d) The orientation of MA^+ dipoles as viewed from *b* axis. The red arrow in panel d denotes the polarization direction.

iodine ions. The Pb ions also show off-center motion within the PbI_6 octahedra; however, the displacement is quite small, on the order of only 0.01 Å. As a consequence of these symmetry-breaking motions of polar molecules and ions, polarization will be induced.

The ferroelectric polarization was calculated via two approaches of the classic point charge model and the Berry phase method.[23,24] In the first approach, we took into account three forms of polarization, which are the orientational polarization of MA^+ dipole ($P_{MA\text{-}O}$),[7,9] the ionic polarization induced by the shift of the positive charge center of MA^+ relative to the negative charge center of the PbI_3^- cage ($P_{MA\text{-}I}$), and the ionic polarization induced by the off-center displacement of Pb within the PbI_6 octahedral (P_{Pb}). The polarization values calculated by the classic point charge model were further verified by the Berry phase method. As can be seen in Table 2, these two calculation methods result in consistent polarization values. The direction of the calculated polarization is visualized in Figure 1d. The magnitude of polarization is only ~8 $\mu C/cm^2$, in which MA^+ groups contribute a major portion. This polarization magnitude is similar to that reported in ref 9, while it is considerably smaller than that reported in ref 7. This discrepancy can well be caused by the off-center motion of Pb, which was claimed by Frost et al.[7] to be very significant and thus could make a pronounced contribution toward the overall polarization. In our calculations and those of other authors,[9,22,25,26] the off-center motion of Pb is quite weak.

Table 2. Polarization of the Most Stable Tetragonal Structure (T-13) of $MAPbI_3$

		polarization ($\mu C/cm^2$)		
method	form of *P*	P_x // [100]	P_y // [010]	P_z // [001]
point charge model	$P_{MA\text{-}O}$[a]	1.86	0	−1.32
	$P_{MA\text{-}I}$	3.66	0	−2.62
	P_{Pb}	0.95	0	−0.25
	P_{total}[b]	6.47	0	−4.19
Berry phase	P_{total}	6.69	0	−4.27

[a] $P_{MA\text{-}O}$, $P_{MA\text{-}I}$, P_{Pb}, and P_{total} denote the orientational polarization of MA^+, ionic polarization of MA^+, ionic polarization of Pb, and total polarization. [b] Because of symmetry, P_{total} can be any one of ($\pm|P_x|$, 0, $\pm|P_z|$) and (0, $\pm|P_y|$, $\pm|P_z|$).

The calculations of polarization deserve some further comments. First, one must bear in mind that the 3-D PBCs are mandatory in DFT calculations; therefore, the calculated polarization, which is a bulk property, may not be applicable to a disordered system. Second, if 3-D PBCs are satisfied, one may also be concerned with the reliability to use DFT calculations, which are performed at zero temperature, to simulate the polarization of the room-temperature tetragonal phase of $MAPbI_3$. Rabe et al.[27] have addressed this concern in their classic book. In addition, many examples of inorganic perovskites[28−31] have confirmed that the DFT calculation can well quantify the polarization of a room-temperature phase, although this phase may not even exist at zero temperature.

Now let us turn to the experimental results of measurements on the possible ferroelectric properties of the $MAPbI_3$ thin film. We first conducted the phase analysis in the thin film. The XRD pattern in Figure S2 (Supporting Information) demonstrates that the tetragonal $MAPbI_3$ phase is crystallized. Moreover, the polycrystalline feature of the $MAPbI_3$ film ensures that if the ferroelectric polarization exists it can be detected along the out-of-plane direction.

Au top electrodes with a diameter of 200 μm were sputtered onto the surface of the film to form a sandwich structure of Au/$MAPbI_3$/PEDOT:PSS/ITO prior to measuring the macroscopic *P*−*E* hysteresis loops. Note that the PEDOT:PSS layer is ultrathin and highly conductive (Figure S3 in Supporting Information); therefore, $MAPbI_3$ is the only measured layer. *P*−*E* loops were measured at room temperature with varying the amplitude and frequency of the applied voltage. As can be seen from Figure 2a,b, neither increasing the voltage amplitude nor decreasing the frequency (i.e., increasing the duration of applied voltage) can result in a *P*−*E* loop with ferroelectric characteristics. The measured polarization is simply dominated by leakage current; therefore, the remnant polarization (excluding leakage contribution) is close to zero. To further prove this viewpoint, the current−electric field (*I*−*E*) hysteresis loop was measured with an applied voltage of 1 V and 10 Hz. As shown in Figure 2c, *I* increases nonlinearly with *E* until it reaches E_{max} (Path 1), while it decreases nonlinearly with *E* until zero field (Path 2). No sign of current peak corresponding to ferroelectric switching is observed. To better understand the characteristic current peak of ferroelectric switching, we used a reference ferroelectric capacitor of Au/$BiFeO_3$/$SrRuO_3$. The *I*−*V* and corresponding *P*−*E* hysteresis loops of Au/$BiFeO_3$/$SrRuO_3$ are presented in Figure 2d. Two current peaks located in the vicinity of coercive field (E_c) are clearly observed, indicating the occurrence of ferroelectric switching. When the ferroelectric switching is completed, although *E* continues to increase, *I* increases only slightly because of small leakage current. (See the end of Path 2 or Path 5 in Figure 2d.) Comparing Figure 2c,d, one can easily see that the room-temperature electric behavior of $MAPbI_3$ is similar to nonlinear resistor-like behavior, which is essentially different from that of the typical ferroelectric perovskite $BiFeO_3$. Therefore, we conclude that $MAPbI_3$ does not exhibit any ferroelectric behavior macroscopically at room temperature. Our findings are consistent with those reported in refs 17 and 32, while they are different from those reported in ref 12. In ref 12, Wei et al.

DOI: 10.1021/acs.jpclett.5b00389
J. Phys. Chem. Lett. 2015, 6, 1155−1161

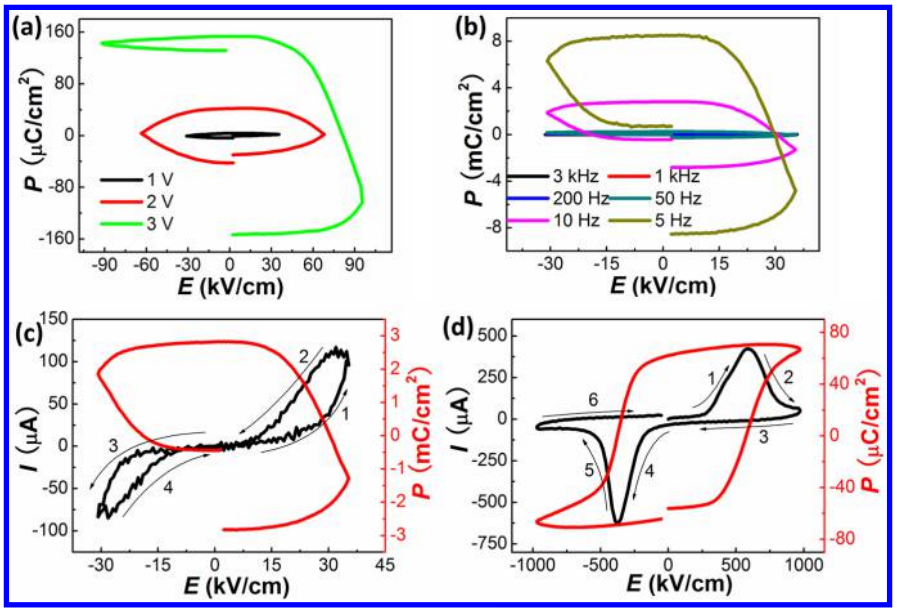

Figure 2. *P*–*E* hysteresis loops of Au/$MAPbI_3$(300 nm thick)/PEDOT:PSS/ITO measured with (a) various voltage amplitudes and a fixed frequency of 3 kHz, and (b) various frequencies and a fixed voltage amplitude of 1 V. (c) I–E and *P*–*E* hysteresis loops of Au/$MAPbI_3$/PEDOT:PSS/ITO measured with an applied voltage of 1 V and 10 Hz. (d) I–E and *P*–*E* hysteresis loops of a reference ferroelectric capacitor of Au/$BiFeO_3$(260 nm thick)/$SrRuO_3$ measured with an applied voltage of 26 V and 1 kHz. The change of *I* in response to *E* follows the path as indicated in panels c and d. The applied electric field in panel c is much smaller than that in panel d because the $MAPbI_3$ sample[12,17,32] is much more leaky compared with the $BiFeO_3$ sample.

observed the nonparabolic shape of the *P*–*E* loop of FTO/Au/Ti/$MAPbI_3$/Al_2O_3/Au and then claimed that it was caused by the ferroelectric behavior of $MAPbI_3$; however, such a nonparabolic shape of *P*–*E* loop may also be resulted from nonlinear leakage behavior.[33] When an insulating Al_2O_3 layer was inserted, it caused even more significant nonlinearity of leakage due to the charge accumulation and release at the $MAPbI_3$/Al_2O_3 interface.

The ferroelectric properties of $MAPbI_3$ were then investigated microscopically by PFM at room temperature. When the positive (negative) DC poling voltage is smaller than +2.5 V (−1.5 V), there are almost no changes of the amplitude and phase images (Figure 3a–f). When the DC poling voltage reaches +2.5 V (−1.5 V), significant changes are observed in amplitude and phase images; however, the simultaneous changes in the topography images (Figure 3a,d) suggest that the observed amplitude and phase changes are not resulted from ferroelectric domain switching but rather associated with electrochemical phenomena.[34] Another way of poling the sample by using small DC voltage (±1 V) with longer duration (i.e., slower poling scan rate) was also tried. Unfortunately, as shown in Figure 3g–i, distinct features of electrochemical phenomena and leakage are observed again. We further probed the possible polarization switching behavior in a more localized region by PFS. As can be seen from Figure S4 (Supporting Information), the amplitude hysteresis loop does not exhibit any butterfly shape, and there is no characteristic 180° phase change. All of the above observations indicate that $MAPbI_3$ is not ferroelectric at room temperature. Our PFM results agree well with those in ref 17, while they contradict those in ref 16. In ref 16, Kutes et al. observed distinct 180° phase change after DC poling; however, the DC voltage applied by them was as large as 8 V, leading to an electric field up to 800 kV/cm. (The thickness was 100 nm.) This large field is far beyond the maximum allowed field for our $MAPbI_3$ film. As pointed out by Kutes et al. in ref 16, a Schottky junction might form between tip and sample, which could share the majority of the applied field. As a result, one could infer that the injected charges within the junction area would strongly affect the phase image if those charges were not properly removed.

While *P*–*E* hysteresis loops and PFM results of the poled samples show no ferroelectric switching behavior for $MAPbI_3$ at room temperature, the question of whether there are local domain-like structures in $MAPbI_3$ has yet to be clarified. We have therefore carefully analyzed the PFM results of the as-grown $MAPbI_3$ samples. As shown in Figure S5 (Supporting Information), the major portion of the phase image shows brown color, while some small regions show dark color, which can, however, be attributed to sample surface-roughness-induced artifacts. (See the detailed discussion in the Supporting Information.) Previously reported phase contrasts in the as-grown $MAPbI_3$ samples may be also associated with the same artifacts because those samples also exhibit large surface roughness.[16] Therefore, as suggested by our PFM results, it is unlikely that domain-like structures exist in $MAPbI_3$, which is consistent with the observation in ref 17. In addition, it is also unlikely that all of the dipoles in the whole scanned area show the same orientation because MA^+ groups, which are the major polarization contributors, exhibit dynamic orientational disorder at room temperature. As has been studied by single crystal X-ray diffraction[18,35,36] and as indicated by the Raman results of our thin film sample (Figure S6 in Supporting Information), the dynamic orientational disorder of MA^+ groups does unambiguously exist at room temperature.

The conclusion drawn from our experimental results is that there is no apparent ferroelectricity in $MAPbI_3$ at room temperature, which is inconsistent with our computational results. Therefore, effort has to be made to explain the discrepancy. The first consideration is that our DFT calculations are based on the 3-D PBCs, assuming that the

DOI: 10.1021/acs.jpclett.5b00389
J. Phys. Chem. Lett. 2015, 6, 1155–1161

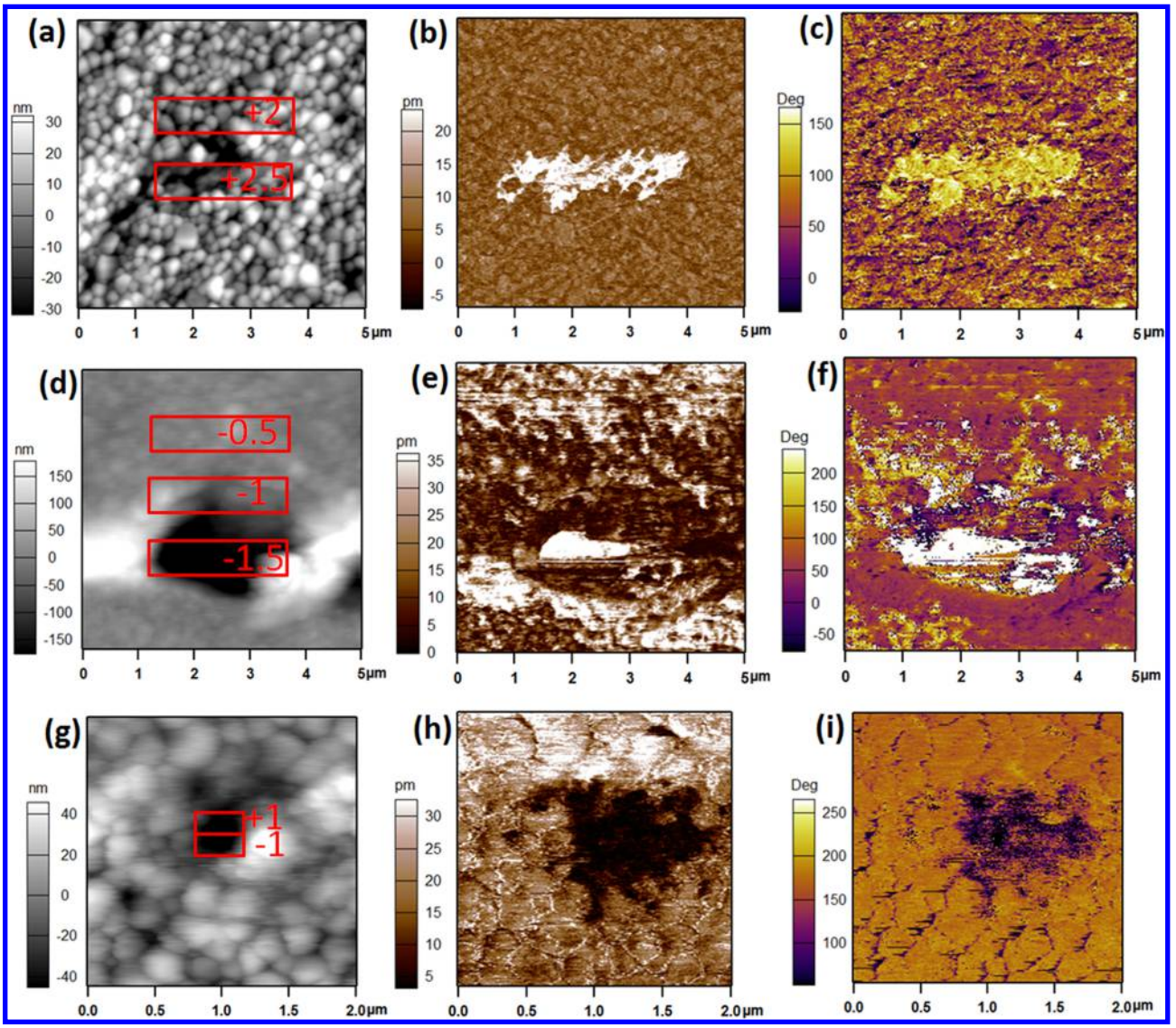

Figure 3. (a) Topography, (b) amplitude, and (c) phase images taken after DC poling with various positive tip biases and a poling scan rate of 0.8 Hz. (d) Topography, (e) amplitude, and (f) phase images taken after DC poling with various negative tip biases and a poling scan rate of 0.8 Hz. (g) Topography, (h) amplitude, and (i) phase images taken after DC poling with ±1 V tip biases and a poling scan rate of 0.1 Hz. All PFM images were taken after poling and subsequent grounded-tip scanning. Poled areas are marked by the red rectangles.

whole $MAPbI_3$ bulk is constructed by repeating the unit cell in three dimensions. However, the dynamic orientational disorder of MA^+ groups makes the 3-D PBCs fail at room temperature. Therefore, although there might be a dipole moment on the unit-cell scale, the random orientations of those dipole moments will lead to an average zero polarization in bulk form. Moreover, our PFM results show that there is no formation of ferroelectric domains, which indicate that the dipole moments cancel each other in a relatively microscopic region. The second consideration is that DFT calculations of polarization assume the system being insulating, while in the real situation, $MAPbI_3$ exhibits semiconducting nature at room temperature. $MAPbI_3$ films contain a large quantity of charge carriers ($>10^{17}$ cm^{-3}) with high mobility[4,37] and have a small energy band gap (1.25 to 1.75 eV),[2] and thus the leakage current is expected to be very high, even under a small electric field. Therefore, although there might be dipoles alignment under electric field, the resulting polarization variation is almost impossible to be observed experimentally with the strong influence of leakage current.

Despite the limitations of the DFT calculations, our results still provide valuable suggestions for future study on the ferroelectricity of $MAPbI_3$. For example, our calculated most stable structure of $MAPbI_3$ and its ferroelectric polarization can be used as the starting point for further finite-temperature simulations.[27,38] In addition, our calculations suggest that if MA^+ groups become ordered with the predicted polar unit cell as the repeating unit of the $MAPbI_3$ crystal, ferroelectric domains will be formed. In this connection, low temperature will be the desirable condition. Moreover, lowering temperature will reduce leakage current, which is favorable for the ferroelectric domain switching. Therefore, it would be of scientific interest to further investigate the ferroelectricity of $MAPbI_3$ at low enough temperatures; however, at low-temperature $MAPbI_3$ may crystallize into an orthorhombic *Pnma* phase,[36] which is centrosymmetric without any ferroelectricity. Recent *P*–*E* measurements conducted at 77 K

DOI: 10.1021/acs.jpclett.5b00389
J. Phys. Chem. Lett. 2015, 6, 1155−1161

showed that there was still no ferroelectric behavior for $MAPbI_3$.[18,32] To induce and experimentally observe the apparent ferroelectricity, several pathways besides further lowering temperature, such as cooling $MAPbI_3$ under electric field or mechanical strain,[22] and substituting iodine with other halogen elements to create distortions for PbX_3 cages and PbX_6 octahedra,[9] can be employed in future studies.

In summary, we have systematically studied the ferroelectricity of $MAPbI_3$ both theoretically and experimentally. Our DFT calculations show that if 3-D PBCs are fulfilled, the most stable tetragonal structure of $MAPbI_3$ is a ferroelectric one. Moreover, the polarization magnitude is calculated to be ~8 $\mu C/cm^2$, which may serve as a benchmark for further investigations; however, both macroscopic $P-E$ hysteresis measurements and microscopic PFM demonstrate that there is no room-temperature ferroelectricity in $MAPbI_3$. The inconsistency between our theoretical and experimental results is well-explained by considering the dynamic orientational disorder of MA^+ groups and the semiconducting nature of $MAPbI_3$ at room temperature. Therefore, we conclude that $MAPbI_3$ is not ferroelectric at room temperature; however, it is promising to induce and experimentally observe apparent ferroelectric behavior of $MAPbI_3$ by a couple of pathways as proposed. Our results clarify the controversy of the ferroelectricity in $MAPbI_3$ and also provide valuable suggestions and guidance for future studies on this active topic.

■ ASSOCIATED CONTENT

Supporting Information

18 possible tetragonal structures of $MAPbI_3$ (Figure S1), XRD pattern of the $MAPbI_3$ thin film (Figure S2), purpose of using PEDOT:PSS buffer layer and evidence of its high conductivity (Figure S3), amplitude and phase hysteresis loop (Figure S4), PFM topography and phase images of as-grown MAPbI3 sample (Figure S5), room-temperature Raman spectrum of the $MAPbI_3$ thin film (Figure S6), and relative energies of all structures calculated with van der Waals corrections (Table S1). This material is available free of charge via the Internet at http://pubs.acs.org.

■ AUTHOR INFORMATION

Corresponding Author

*E-mail: msewangj@nus.edu.sg.

Notes

The authors declare no competing financial interest.

■ ACKNOWLEDGMENTS

Z.F. and J.W. acknowledge the support from the Agency for Science, Technology and Research (A*Star) for research (grant no. 1121202013), conducted at the National University of Singapore.

■ REFERENCES

(1) Jeon, N. J.; Noh, J. H.; Yang, W. S.; Kim, Y. C.; Ryu, S.; Seo, J.; Seok, S., II. Compositional Engineering of Perovskite Materials for High-Performance Solar Cells. *Nature* **2015**, *517*, 476−480.

(2) Stoumpos, C. C.; Malliakas, C. D.; Kanatzidis, M. G. Semiconducting Tin and Lead Iodide Perovskites with Organic Cations: Phase transitions, High mobilities, and Near-Infrare Photoluminescent Properties. *Inorg. Chem.* **2013**, *52*, 9019−9038.

(3) Takahashi, Y.; Hasegawa, H.; Takahashi, Y.; Inabe, T. Hall Mobility in Tin Iodide Perovskite CH_3NH_3/SnI_3: Evidence for a Doped Semiconductor. *J. Solid State Chem.* **2013**, *205*, 39−43.

(4) Wehrenfennig, C.; Eperon, G. E.; Johnston, M. B.; Snaith, H. J.; Herz, L. M. High Charge Carrier Mobilities and Lifetimes in Organolead Trihalide Perovskites. *Adv. Mater.* **2013**, *26*, 1584−1589.

(5) Xing, G.; Mathews, N.; Sun, S.; Lim, S. S.; Lam, Y. M.; Graetzel, M.; Mhaisalkar, S.; Sum, T. C. Long-Range Balanced Electron- and Hole-Transport Lengths in Organic-Inorganic $CH_3NH_3PbI_3$. *Science* **2013**, *342*, 344−347.

(6) Edri, E.; Kirmayer, S.; Mukhopadhyay, S.; Gartsman, K.; Hodes, G.; Cahen, D. Elucidating the Charge Carrier Separation and Working Mechanism of $CH_3NH_3PbI_{3-x}Cl_x$ Perovskite Solar Cells. *Nat. Commun.* **2014**, *5*, 3461.

(7) Frost, J. M.; Butler, K. T.; Brivio, F.; Hendon, C. H.; van Schilfgaarde, M.; Walsh, A. Atomistic Origins of High-Performance in Hybrid Halide Perovskite Solar Cells. *Nano Lett.* **2014**, *14*, 2584−2590.

(8) Liu, S.; Zheng, F.; Koocher, N. Z.; Takenaka, H.; Wang, F.; Rappe, A. M. Ferroelectric Domain Wall Induced Band Gap Reduction and Charge Separation in Organometal Halide Perovskites. *J. Phys. Chem. Lett.* **2015**, *6*, 693−699.

(9) Zheng, F.; Takenaka, H.; Wang, F.; Koocher, N. Z.; Rappe, A. M. First-Priciples Calculation of the Bulk Photovoltaic Effect in $CH_3NH_3PbI_3$ and $CH_3NH_3PbI_{3-x}Cl_x$. *J. Phys. Chem. Lett.* **2015**, *6*, 31−37.

(10) Unger, E. L.; Hoke, E. T.; Bailie, C. D.; Nguyen, W. H.; Bowring, A. R.; Heumuller, T.; Christoforo, M. G.; McGehee, M. D. Hysteresis and Transient Behavior in Current-Voltage Measurements of Hybrid-Perovskite Absorber Solar Cells. *Energy Environ. Sci.* **2014**, *7*, 3690−3698.

(11) Chen, H.-W.; Sakai, N.; Ikegami, M.; Miyasaka, T. Emergence of Hysteresis and Transient Ferroelectric Response in Organo-Lead Halide Perovskite Solar Cells. *J. Phys. Chem. Lett.* **2015**, *6*, 164−169.

(12) Wei, J.; Zhao, Y.; Li, H.; Li, G.; Pan, J.; Xu, D.; Zhao, Q.; Yu, D. Hysteresis Analysis Based on the Ferroelectric Effect in Hybrid Perovskite Solar Cells. *J. Phys. Chem. Lett.* **2014**, *5*, 3937−3945.

(13) Snaith, H. J.; Abate, A.; Ball, J. M.; Eperon, G. E.; Leijtens, T.; Noel, N. K.; Stranks, S. D.; Wang, J. T. W.; Wojuciechowski, K.; Zhang, W. Anomalous Hysteresis in Perovskite Solar Cells. *J. Phys. Chem. Lett.* **2014**, *5*, 1511−1515.

(14) Shao, Y.; Xiao, Z.; Bi, C.; Yuan, Y.; Huang, J. Origin and Elimination of Photocurrent Hysteresis by Fullerene Passivation in $CH_3NH_3PbI_3$ Planar Heterojunction Solar Cells. *Nat. Commun.* **2014**, *5*, 5784.

(15) Dualeh, A.; Moehl, T.; Tétreault, N.; Teuscher, J.; Gao, P.; Nazeeruddin, M. K.; Grätzel, M. Impedance Spectroscopic Analysis of Lead Iodide Perovskite-Sensitized Solid-State Solar Cells. *ACS Nano* **2014**, *8*, 362−373.

(16) Kutes, Y.; Ye, L.; Zhou, Y.; Pang, S.; Huey, B. D.; Padture, N. P. Direct Observation of Ferroelectric Domains in Solution-Processed $CH_3NH_3PbI_3$ Perovskite Thin Films. *J. Phys. Chem. Lett.* **2014**, *5*, 3335−3339.

(17) Xiao, Z.; Yuan, Y.; Shao, Y.; Wang, Q.; Dong, Q.; Bi, C.; Sharma, P.; Gruverman, A.; Huang, J. Giant Switchable Photovoltaic Effect in Organometal Trihalide Perovskite Devices. *Nat. Mater.* **2015**, *14*, 193−198.

(18) Kawamura, Y.; Mashiyama, H.; Hasebe, K. Structural Study on Cubic−Tetragonal Transition of $CH_3NH_3PbI_3$. *J. Phys. Soc. Jpn.* **2002**, *71*, 1694−1697.

(19) Note that in this work we focus on tetragonal structures of $MAPbI_3$ because they are favored at room temperature.[2,18]

(20) Perdew, J. P.; Ruzsinszky, A.; Csonka, G. I.; Vydrov, O. A.; Scuseria, G. E.; Constantin, L. A.; Zhou, X.; Burke, K. Restoring the Density-Gradient Expansion for Exchange in Solids and Surfaces. *Phys. Rev. Lett.* **2008**, *100*, 136406.

(21) Sun, K.; Chang, J.; Isikqor, F. H.; Li, P.; Ouyang, J. Efficiency Enhancement of Planar Perovskite Solar Cells by Adding Zwitterion/LiF Double Interlayers for Electron Collection. *Nanoscale* **2015**, *7*, 896−900.

DOI: 10.1021/acs.jpclett.5b00389
J. Phys. Chem. Lett. 2015, 6, 1155−1161

(22) Ong, K. P.; Goh, T. W.; Xu, Q.; Huan, A. Mechanical Origin of the Structural Phase Transition in Methylammonium Lead Iodide $CH_3NH_3PbI_3$. *J. Phys. Chem. Lett.* **2015**, *6*, 681−685.
(23) King-Smith, R. D.; Vanderbilt, D. Theory of Polarization of Crystalline Solids. *Phys. Rev. B* **1993**, *47*, 1651−1654.
(24) Vanderbilt, D.; King-Smith, R. D. Electric Polarization as a Bulk Quantity and its Relation to Surface Charge. *Phys. Rev. B* **1993**, *48*, 4442−4455.
(25) Geng, W.; Zhang, L.; Zhang, Y.-N.; Lau, W.-M.; Liu, L.-M. First-Principles Study of Lead Iodide Perovskite Tetragonal and Orthorhombic Phases for Photovoltaics. *J. Phys. Chem. C* **2014**, *118*, 19565−19571.
(26) Umari, P.; Mosconi, E.; Angelis, F. D. Relativistic GW Calculations on $CH_3NH_3PbI_3$ and $CH_3NH_3SnI_3$ Perovskites for Solar Cell Applications. *Sci. Rep.* **2014**, *4*, 4467.
(27) Rabe, K. M.; Ahn, C. H.; Triscone, J. M. *Physics of Ferroelectrics: a Modern Perspective*; Springer: New York, 2007; Vol. *105*, pp 53−54.
(28) Resta, R.; Posternak, M.; Baldereschi, A. Towards a Quantum Theory of Polarization in Ferroelectrics: the Case of $KNbO_3$. *Phys. Rev. Lett.* **1993**, *70*, 1010−1013.
(29) Fu, X.; Cohen, R. E. Polarization Rotation Mechanism for Ultrahigh Electromechanical Response in Single-Crystal Piezoelectrics. *Nature* **2000**, *403*, 281−283.
(30) Neaton, J. B.; Ederer, C.; Waghmare, U. V.; Spaldin, N. A.; Rabe, K. M. First-Principles Study of Spontaneous Polarization in Multiferroic $BiFeO_3$. *Phys. Rev. B* **2005**, *71*, 014113.
(31) Fan, Z.; Xiao, J.; Liu, H.; Yang, P.; Ke, Q.; Ji, W.; Yao, K.; Ong, K. P.; Zeng, K. Y.; Wang, J. Stable Ferroelectric Perovskite Structure with Giant Axial Ratio and Polarization in Epitaxial $BiFe_{0.6}Ga_{0.4}O_3$ Thin Films. *ACS Appl. Mater. Interfaces* **2015**, *7*, 2648−2653.
(32) Zhao, Y.; Liang, C.; Zhang, H.; Li, D.; Tian, D.; Li, G.; Jing, X.; Zhang, W.; Xiao, W.; Liu, Q.; Zhang, F.; He, Z. Anomalously Large Interface Charge in Polarity Switchable Photovoltaic Devices: an Indication of Mobile Ions in Organic−Inorganic Halide Perovskites. *Energy Environ. Sci.* **2015**, DOI: 10.1039/c4ee04064c.
(33) Dawber, M.; Rabe, K. M.; Scott, J. F. Physics of Thin-Film Ferroelectric Oxides. *Rev. Mod. Phys.* **2005**, *77*, 1083−1130.
(34) Kalinin, S. V.; Jesse, S.; Tselev, A.; Baddorf, A. P.; Nina, B. The Role of Electrochemical Phenomena in Scanning Probe Microscopy of Ferroelectric Thin Films. *ACS Nano* **2011**, *5*, 5683−5691.
(35) Poglitsch, A.; Weber, D. Dynamic Disorder in Methylammoniumtrihalogenoplumbates (II) Observed by Millimeterwave Spectroscopy. *J. Chem. Phys.* **1987**, *87*, 6373−6378.
(36) Baikie, T.; Fang, Y.; Kadro, J. M.; Schreyer, M.; Wei, F.; Mhaisalkar, S. G.; Graetzel, M.; White, T. J. Synthesis and Crystal Chemistry of the Hybrid Perovskite $(CH_3NH_3)PbI_3$ for Solid-State Sensitised Solar Cell Applications. *J. Mater. Chem. A* **2013**, *1*, 5628−5641.
(37) Wang, Q.; Shao, Y.; Xie, H.; Lyu, L.; Liu, X.; Gao, Y.; Huang, J. Qualifying composition dependent p and n Self-doping in $CH_3NH_3PbI_3$. *Appl. Phys. Lett.* **2014**, *105*, 163508.
(38) Frost, J. M.; Butler, K. T.; Walsh, A. Molecular Ferroelectric Contributions to Anomalous Hysteresis in Hybrid Perovskite Solar Cells. *APL Mater.* **2014**, *2*, 081506.

DOI: 10.1021/acs.jpclett.5b00389
J. Phys. Chem. Lett. 2015, 6, 1155−1161